

# Trajectory-aware Communication Solution for Underwater Gliders using WHOI Micro-Modems

Baozhi Chen, Patrick C. Hickey, and Dario Pompili

Department of Electrical and Computer Engineering, Rutgers University, Piscataway, NJ 08854

Emails: baozhi\_chen@cac.rutgers.edu, pchickey@eden.rutgers.edu, pompili@ece.rutgers.edu

**Abstract**—The predictable trajectory of underwater gliders can be used in geographic routing protocols. Factors such as drifting and localization errors cause uncertainty when estimating a glider’s trajectory. Existing geographic routing protocols in underwater networks generally assume the positions of the nodes are accurately determined by neglecting position uncertainty. In this paper, a paradigm-changing geographic routing protocol that relies on a statistical approach to model position uncertainty is proposed. Our routing protocol is combined with practical cross-layer optimization to minimize energy consumption. Our solution’s performance is tested and compared with existing solutions using a real-time testbed emulation that uses underwater acoustic modems.

## I. INTRODUCTION

UnderWater Acoustic Sensor Networks (UW-ASNs) [1] have been widely deployed to carry out collaborative monitoring tasks including oceanographic data collection, disaster prevention, and navigation. Autonomous Underwater Vehicles (AUVs) equipped with sensors are used for underwater exploration and information gathering. Underwater gliders are battery powered AUVs that change their buoyancy with hydraulic pumps to power forward motion. These gliders rely on local intelligence with minimal onshore operator dependence. Acoustic communications are used to transfer information (data and configuration) between gliders and finally to a surface station where the data is gathered and analyzed.

Gliders follow sawtooth trajectories, which can be used to predict position and, therefore to improve communications. This position information is used in underwater geographic routing protocols such as [2], [3], which assume the positions of the nodes are known. These protocols do not assume sawtooth trajectory when making routing decisions. Drifting and self localization errors will degrade the network’s estimates of relative glider position, which may lead to inefficient geographic forwarding and even routing failure as shown in papers on terrestrial networking such as [4], [5].

To better handle location uncertainty, in this work we adopt a statistical approach to predict glider positions. We describe glider position with a confidence region instead of a single point. The routing protocol is designed to send packets to a region rather than to a point. To improve the network’s energy efficiency, we adopt a practical cross-layer design that takes advantage of all possible functionalities of the WHOI Micro-Modem [6]. Existing geographic routing protocols usually forward packets to the next hop assuming the exact positions of the nodes are known. In this paper, we employ statistical

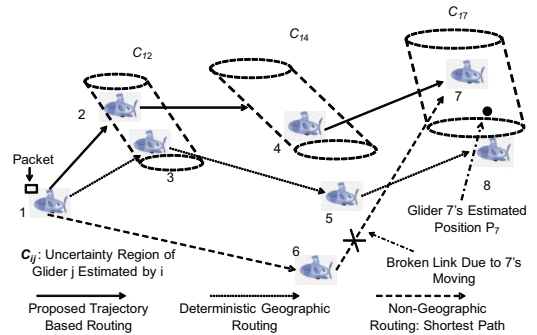


Fig. 1. Comparison of routing protocols.

methods to characterize the location uncertainty and propose a novel solution to improve network performance under such an environment.

By describing each node using a confidence region, our routing algorithm is able to increase the probability of successful packet delivery. To illustrate one way this approach is a better solution than deterministic geographic routing and non-geographic routing protocols, an example is shown in Fig. 1, where glider 1 has a packet to forward to glider 7. Suppose the estimated position of glider 7 is at  $P_7$  with corresponding uncertain region  $C_{17}$ , as seen by glider 1. With our statistical protocol, the packet is estimated by 1 to follow the path  $1 \rightarrow C_{12} \rightarrow C_{14} \rightarrow C_{17}$  and hence can reach glider 7 as 7 is in  $C_{17}$ . On the other hand, with the deterministic geographic routing, the packet may follow the path  $1 \rightarrow 3 \rightarrow 5 \rightarrow 8$  since glider 8 is closer to  $P_7$  than glider 7, and it may not be able to reach 7 with shortest path routing ( $1 \rightarrow 6 \rightarrow 7$ ) as 7 moves out of glider 6’s range.

The contribution of this paper is as follows:

- We propose an approach that uses a statistical region to characterize the glider’s position and design a corresponding routing algorithm. To the best of our knowledge, it is the first geographic routing protocol using statistical methods to describe location uncertainty for UW-ASNs.
- We develop a unicast routing protocol that automatically provides a solution for *geocasting*, which routes packets to all the gliders within a specific geographic region.
- We provide a practical cross-layer optimization solution that exploits the functionalities of the WHOI Acoustic Micro-Modem to minimize energy consumption. Our solution has been implemented and tested in our underwater

testbed, which can better emulate underwater communications than existing testbeds.

The remainder of this paper is organized as follows. In Sect. II, we review the related work for geographic routing in UW-ASNs. We present the underwater communication model in Sect. III and proposed solution in Sect. IV, followed by the emulation testbed in Sect. V. In Sect. VI, performance evaluation and analysis are carried out, while conclusions are discussed in Sect. VII.

## II. RELATED WORK

Geographic routing protocols, e.g., Greedy-Face-Greedy (GFG) [7] and Partial Topology Knowledge Forwarding (PTKF) [8], are very promising because of their scalability and limited signaling requirement. However, Global Positioning System (GPS) radio receivers, which may be used in terrestrial systems to accurately estimate the geographic location of sensor nodes, do not work properly in the underwater environment. GPS uses waves in the 1.5 GHz band which do not propagate in water. Underwater devices (sensors, AUVs, etc.) need to estimate their position for association with sampled data. Underwater localization can be achieved by leveraging the low speed of sound in water, which permits accurate timing of signals. Measured pairwise node distance can be used to perform 3D localization, similar to the 2D localization demonstrated in [9].

In [2], a geographic routing protocol based on Dynamic Source Routing (DSR) with location awareness is proposed. It employs the range information to estimate local network topology, showing improved network capacity over blind flooding and DSR protocols as node distance becomes large. Focus Beam Routing (FBR) protocol [3] employs a directional beam-forming technique with the help of location information for packet forwarding. It is shown that FBR has energy consumption performance close to Dijkstra’s algorithm while additional burden of dynamic route discovery is minimal.

A cross-layer optimization solution for UW-ASNs has been proposed in [10], where interaction between routing functions and underwater characteristics is exploited, resulting in improvement in end-to-end network performance in terms of both energy and throughput. A study on the interaction between physical and MAC layers is presented in [11], where a method is proposed to estimate the battery lifetime and power cost for shallow water underwater acoustic sensor networks. In this way, the energy consumption is equalized and the network lifetime is prolonged. A cross-layer approach that jointly considers the routing protocol, the medium access control, and the physical layer functionalities is proposed in [3], showing improved energy consumption performance. These solutions are implemented and tested only by software simulation platforms. On the contrary, we propose a practical cross-layer solution that incorporates the functionalities of the WHOI Micro-Modem to minimize energy consumption; also our solution is implemented on real hardware and tested in our emulation testbed.

## III. NETWORK MODEL

In this section we introduce the UW-ASN that our proposal is based on and state the related assumptions. Suppose the network is composed of a number of gliders that will forward data to a glider that collects data. Gliders are deployed in the ocean for long periods (weeks to months) of time to collect oceanographic data. For propulsion, they change their buoyancy using a pump, and let foils provide forward motion as they rise and fall through the ocean. They travel at a fairly constant horizontal speed, typically 0.25 m/s [1]. Gliders control their heading towards predefined waypoints using a magnetic compass. This slow and predictable trajectory is used in our proposal to estimate another glider’s position using its own position and velocity estimate from some time earlier. A glider’s own position and velocity is sent to neighboring gliders. But, for efficiency, only every other estimate is forwarded to non-neighboring gliders. Sufficient information is provided in an estimate to extrapolate a glider’s current position, and a confidence region accounts for possible deviation from the extrapolated course.

The Urick model is a coarse approximation for underwater acoustic wave propagation, whose transmission loss  $TL(l, f)$  [dB] can be model as,

$$TL(l, f) = \kappa \cdot 10\log(l) + \alpha(f) \cdot l, \quad (1)$$

where  $l$  is the distance between the transmitter and receiver and  $f$  is the carrier frequency. Spreading factor  $\kappa$  is taken to be 1.5 for practical spreading, and  $\alpha(f)$  [dB/m] represents an absorption coefficient that increases with  $f$  [12].

In reality, sound propagation speed varies with water temperature, salinity, and pressure, which causes wave paths to bend. Acoustic waves are also reflected from the surface and bottom. Such uneven propagation of waves results in convergence (or shadow) zones which may receive much less (or more) transmission loss than that predicted by the Urick model. Due to space limitation, we cannot give a detailed description, but more details can be found in [13].

Due to these phenomena, the Urick model is not sufficient to describe the underwater channel for simulation purposes. The Bellhop model is based on ray/beam tracing, which can model these phenomena more accurately. This model can estimate the transmission loss by two-dimensional acoustic ray tracing for a given sound speed depth profile or a given sound speed field, in ocean waveguides with flat or variable absorbing boundaries. Transmission loss is calculated by solving differential ray equations, and a numerical solution is provided by HLS Research [14]. Because the Bellhop model requires more information about the environment than a glider will have, it is only used to simulate the acoustic environment for testing. The proposed cross-layer optimization uses the Urick model in the cross-layer optimization (Sect. IV-C) so that it may be computed on the glider.

We adopt the empirical ambient noise model presented in [12], where a ‘V’ structure of the power spectrum density (psd) is shown. The ambient noise power is obtained by integrating the empirical psd over the frequency band in use. Note that

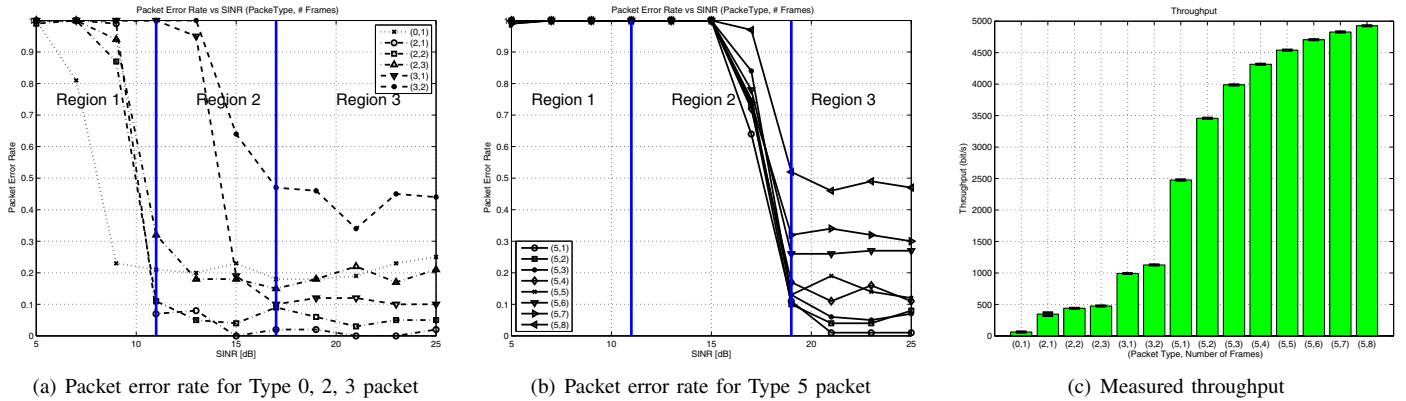


Fig. 2. Measured packet error rate and throughput.

TABLE I  
4 TYPES OF PACKETS USED BY WHOI ACOUSTIC MICRO-MODEM [15]

Type <sup>1</sup>	Modulation	Coding Scheme	bps	Max. Frames	Frame Bytes
0	FH-FSK		80	1	32
2	PSK	1/15 spding <sup>2</sup>	500	3	64
3	PSK	1/7 spding	1200	2	256
5	PSK	9/17 RBC <sup>3</sup>	5300	8	256

<sup>1</sup> Type 1 and 4 are unimplemented; <sup>2</sup> i.e., “spreading”; <sup>3</sup> i.e., “Rate Block Code”.

in underwater acoustics, power (or source level) is usually expressed using decibel (dB) scale, relative to the reference pressure level in underwater acoustics  $1\mu Pa$ , i.e., the power (or source intensity) induced by  $1\mu Pa$  pressure. The conversion expression for the source level  $SL$  re  $\mu Pa$  at the distance of 1 m of a compact source of  $P$  watts is shown in [13] as  $SL = 170.77 + 10 \log P$ .

#### IV. PROPOSED APPROACH

In this section, our proposed approach is presented by first introducing the motivation for cross-layer optimization with the statistical approach, followed by the description of the statistical region estimation for gliders and finally the cross-layer design of our proposed protocols.

##### A. Motivation

Underwater channel is characterized by high and variable propagation delay, limited bandwidth capacity, frequency dependent attenuation, noise, fading, and Doppler spread. Due to these unique characteristics, we adopt a cross-layer design approach, which has been shown to be necessary [10].

Our proposed solution is based on the WHOI Micro-Modem. To exploit its functionalities, we first test the Signal-to-Interference-plus-Noise Ratio (SINR) performance of the Micro-Modem with our testbed. As Bit Error Rate (BER) can not be directly measured, we use the measured Packet Error Rate (PER) versus SINR figure to characterize the modem’s communication performance in real underwater environment.

As shown in Table I, there are 4 types of packets using different modulation and coding schemes. Each packet is divided into

a number of frames  $N_F$  depending on its packet type. The PER of each packet type at each frame length is shown in Figs. 2(a) and 2(b). As we can see in Fig. 2(a), in the low SINR region (Region 1:  $< 11$ dB), the PER relationship between different types are: Type 0 < Type 2 < Type 3.

Note that: i) as  $SINR > 11$ dB (Region 2 and 3), Type 2 packet has lower PER than Type 0; Type 2 packet with 3 frames has about the same PER as Type 0, but its bit rate is much higher than Type 0; ii) Type 3 packet with 1 frame has approximately the same PER as Type 0, but the bit rate is much higher.

As for Type 5 packet (Fig. 2(b)), when  $SINR < 17$ dB (Region 1 and 2), its PER is higher than the other packet types. For  $SINR > 17$ dB (Region 3), it has very good PER performance. It has the highest bit rate of 5300 bps.

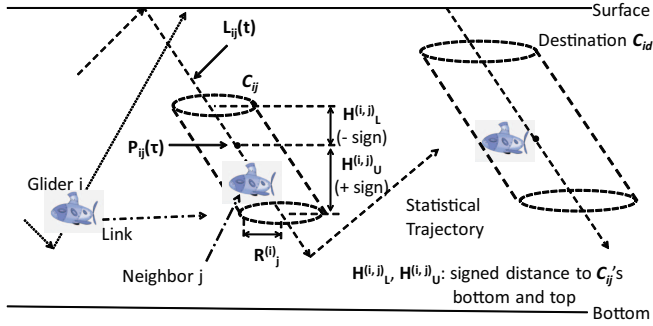
As shown in Fig. 2(c), as  $N_F$  increases, measured throughput increases along with the PER. Different types of packets have different PER for a specific SINR. Therefore the protocol must balance the tradeoff between PER and throughput with a joint consideration of packet type and  $N_F$ .

##### B. Unicast Region Estimation

In this paper, we exploit the glider’s predictable sawtooth trajectory in the routing algorithm. Each glider’s own velocity and position estimate, along with the sawtooth trajectory assumption, is used to determine a confidence region of that glider’s position by each other glider. Packets are routed to the best neighboring region given the estimated regions for the destination and each neighboring node.

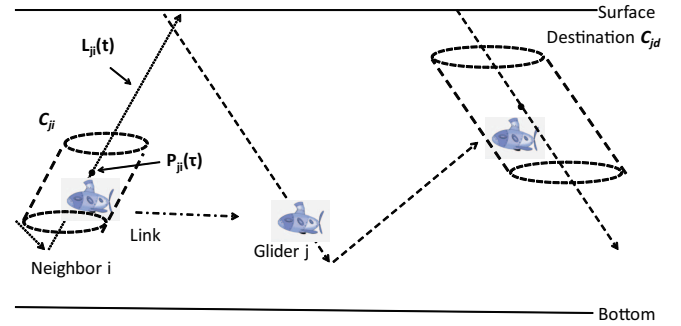
In this subsection, we focus on estimating the possible regions that the gliders are in with statistical methods and leave the problem of selecting the best neighbor for packet forwarding to the next subsection. After the regions of the gliders are estimated, the unicast networking problem becomes a geocasting problem.

As shown in Fig. 3, we assume each glider follows a sawtooth trajectory composed of line segments (possible as shown in [16]). Each glider is assumed to be randomly deployed in a 3D region and glides up or down with the same absolute *vertical angle*, i.e., the vertical angle of the glider’s trajectory in range



Estimations to  $j$  by  $i$ :  $C_{ij}$  - Uncertainty Region;  $L_{ij}(t)$  - Line Segment;  $P_{ij}(t)$  - Centroid.

(a) Estimated regions by  $i$ : a cylinder with circular bottom radius  $R_U^{(i,j)}$  and height  $H_U^{(i,j)} - H_L^{(i,j)}$ .



Estimations to  $i$  by  $j$ :  $C_{ji}$  - Uncertainty Region;  $L_{ji}(t)$  - Line Segment;  $P_{ji}(t)$  - Centroid.

(b) Estimated regions by  $j$ . Note that  $C_{jd}$  for  $d$  may be different from that  $C_{id}$  in Fig. 3(a) as every glider has its own estimation for others regions.

Fig. 3. Each glider estimates other gliders' trajectories and regions.

$[-\pi/2, \pi/2]$  with respect to the  $x$ - $y$  plane. Furthermore, we assume that the glider will continue at the same heading on the  $x$ - $y$  plane. Each moves between two horizontal boundary planes; a glider keeps moving in its current direction until it reaches a boundary plane, where it will change its pitch and move towards the other boundary plane with the same absolute vertical angle. These assumptions are made to simplify calculations so that we can focus on the main problems, and can be changed later without significant consequence to our algorithm.

Whenever glider  $i$  has a packet to forward, it estimates the regions of its neighbors and that of the destined glider  $d$ , selects the best neighbor  $j$  and forwards the packet to  $j$ 's region.

To offer glider  $i$  the information for region estimation, every  $\Delta$  seconds, glider  $j$  broadcasts its velocity information  $\vec{v}_n$ , next turning points, and destined location, where  $n = 1, 2, \dots$  is the time index. Upon receiving this message,  $i$  can estimate  $j$ 's next location coordinates  $loc_n(x_n, y_n, z_n)$  by  $loc_n = loc_{n-1} + \vec{v}_n \Delta$ . The effect of  $\Delta$  on the estimated region is shown in Fig. 4(a). Here we assume the initial position  $loc_0$  (e.g., initial deployment position on the surface) of  $j$  is known to the receiving glider. If the message is lost during transmission, the location is updated with the last available velocity. Consequently, the estimated regions may be different for different estimating gliders.

The glider also broadcasts the location information from the neighbors. To reduce the overhead, it sends out location information from the neighbors every  $2\Delta$  seconds. Therefore, location information of the  $k$ -th hop will be broadcast every  $2^k \Delta$  seconds. Each glider follows its own clock to broadcast so network wide synchronization is not necessary. Existing geographic routing protocols usually require location information of remote nodes to be updated timely to avoid routing failure, while our solution reduce such requirement by using uncertainty region. Therefore, the location overhead is reduced.

Assume glider  $i$  stores all the previous geographic locations  $loc_n$ 's of glider  $j$  up to index  $N$  for  $j$ 's current trajectory line. To estimate  $j$ 's region,  $i$  follows two steps with the help of statistical methods:

- *Step 1*, estimate  $j$ 's trajectory with statistical regression

methods.

- *Step 2*, based on the estimated trajectory, estimate the cylindrical confidence region  $C_{ij}$  in which  $j$  is currently located with a specified confidence  $(1 - \alpha)^2$ .

Note that the confidence region is taken to be cylindrical assuming the ideal current model where the current is depth independent: as glider  $j$  moves, it deviates from the planned trajectory under the influence of current. As  $i$  generally has no information about the current affecting  $j$ ,  $j$ 's deviation is random for  $i$ . If the ocean current moves in any direction in the 3D space,  $j$ 's drifting can be treated as a 3D Brownian Motion where the deviations in  $x$  and  $y$  direction are identically independently distributed (i.i.d.), which makes the horizontal projection of  $j$ 's confidence region circular. And as  $j$  moves along its ascending or descending trajectory, the region swept is a cylinder. Although the pressure sensor on  $j$  gives a rather accurate vertical location, there still can be vertical uncertainty due to upwelling or downwelling currents. This assumption can be made more realistic with better shape modeling according to the ocean current model in use, which is left as future work, but the overall approach would stay the same.

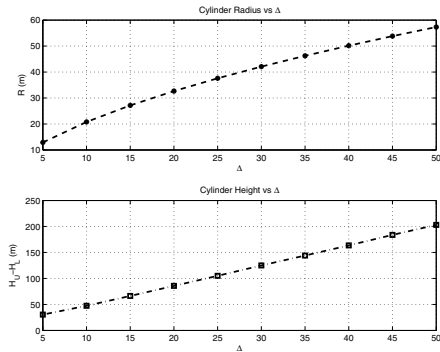
From statistics, the Orthogonal Least Square (OLS) line gives the best maximum likelihood estimation [17]. In other words, the regression line  $(x_0 + at, y_0 + bt, z_0 + ct)$  is the best fitting line such that the sum of the squared distances between it and  $loc_n$ 's is minimal. Here  $x_0, y_0, z_0, a, b, c$  are coefficients to be calculated while  $t$  is the real-valued variable for this parameterized line.

As shown in Fig. 4(b), denote the distance of  $loc_n$  to the regression line by  $d_n$ , OLS regression gives a line that minimizes the sum of the squared distances, i.e., it minimizes

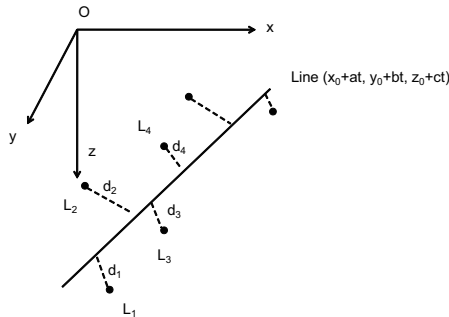
$$f(x_0, y_0, z_0, a, b, c) = \sum_{n=1}^N d_n^2. \quad (2)$$

From geometry, it is not hard to derive

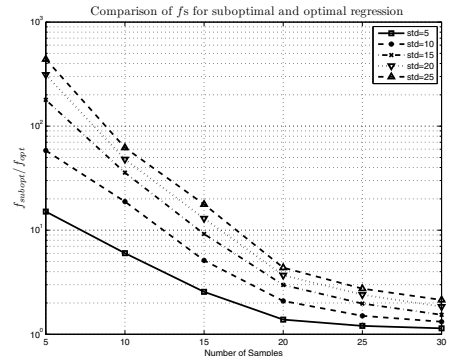
$$d_n^2 = \{[c(y_n - y_0) - b(z_n - z_0)]^2 + [a(z_n - z_0) - c(x_n - x_0)]^2 + [b(x_n - x_0) - a(y_n - y_0)]^2\} / (a^2 + b^2 + c^2). \quad (3)$$



(a) Estimated cylinder region for  $\alpha = 0.05$ : the larger the update interval  $\Delta$  is, the bigger the estimated region is.



(b) Estimated line.



(c) Comparison of suboptimal and optimal solution:  $f_{subopt}$  and  $f_{opt}$  are the minimal values of the suboptimal and optimal solution, respectively.

Fig. 4. Estimation of glider's trajectory and region.

As a consequence, the following equations must be satisfied,

$$\frac{\partial f}{\partial x_0} = \frac{\partial f}{\partial y_0} = \frac{\partial f}{\partial z_0} = \frac{\partial f}{\partial a} = \frac{\partial f}{\partial b} = \frac{\partial f}{\partial c} = 0. \quad (4)$$

However, this equation group is a cubic equation group with 6 variables for which it is hard to derive a closed-form solution.

To reduce the complexity of this problem, we divide it into two sub-problems by the observation from (3) that  $x_0, y_0, z_0$  and  $a, b, c$  have similar effect on  $d_i$ . Therefore, our *first sub-problem* is to find the  $x_0^*, y_0^*, z_0^*$  that minimize  $f$  by assuming  $a, b, c$  are known. Then, based on the solution on the first problem, i.e.,  $(x_0^*, y_0^*, z_0^*)$ , we will find the optimal  $a^*, b^*, c^*$  which can minimize  $f$  (*second sub-problem*).

Solutions for these two sub-problems are provided in [18], which shows that  $[x_0^*, y_0^*, z_0^*] = [\bar{x}, \bar{y}, \bar{z}]$  and  $[a^*, b^*, c^*]^T$  is the corresponding eigenvector to the maximum eigenvalue  $\lambda_{max}$  of  $\mathbf{A}^T \mathbf{A}$ , where  $\bar{x} = \frac{1}{N} \sum_{n=1}^N x_n$ ,  $\bar{y} = \frac{1}{N} \sum_{n=1}^N y_n$ ,  $\bar{z} = \frac{1}{N} \sum_{n=1}^N z_n$ , and

$$\mathbf{A} = \begin{bmatrix} x_1 - \bar{x} & y_1 - \bar{y} & z_1 - \bar{z} \\ x_2 - \bar{x} & y_2 - \bar{y} & z_2 - \bar{z} \\ \vdots & \vdots & \vdots \\ x_N - \bar{x} & y_N - \bar{y} & z_N - \bar{z} \end{bmatrix}.$$

Computation complexity for  $[a^*, b^*, c^*]^T$  can be further reduced by the following proposition.

*Proposition 1:*  $[a^*, b^*, c^*]^T$  is the singular vector of  $\mathbf{A}$  corresponding to its largest absolute singular value. (see Appendix)

With this regression line,  $j$ 's expected position  $P_{ij}(\tau)$  for the time  $\tau$  can thus be estimated from this line (even if there are turns). The optimal and sub-optimal solutions with two sub-problems are compared in Fig. 4(c), where *std* is the standard deviation of the samples from trajectory. When  $N$  is small, the optimal solution gives a better fitting line. As  $N$  gets larger,  $f_{opt}$  and  $f_{subopt}$  get closer; yet, the suboptimal solution gives an algorithm that requires much less computation (see Appendix).

Based on this regression line, we derive the confidence region (the unicast region)  $\mathcal{C}_{ij}$  with radius  $R_j^{(i)}$  and height  $H_U^{(i,j)} - H_L^{(i,j)}$  as shown in Fig. 3. Here,  $H_U^{(i,j)}$  and  $H_L^{(i,j)}$  are *signed distance* of the cylinder's top and bottom surface

to glider  $j$ 's expected location  $P_{ij}(\tau)$  at time  $\tau$ . By signed distance, we mean that the distance is negative if it falls behind  $P_{ij}(\tau)$  in glider  $j$ 's moving direction, and positive if ahead. For convenience,  $H_U^{(i,j)}$ ,  $H_L^{(i,j)}$ , and  $R_j^{(i)}$  are denoted by  $H_U$ ,  $H_L$ , and  $R$ , respectively.

Denote glider  $j$ 's actual position by  $Q_j(\tau)$ . Let  $D$  be the *horizontal distance* of  $Q_j(\tau)$  to  $j$ 's current trajectory line and  $H$  be the *vertical signed distance* of  $Q_j(\tau)$  to the horizontal cross section of  $\mathcal{C}_{ij}$  that passes through  $P_j(\tau)$ .

The problem to jointly find the  $H_L, H_U$ , and  $R$  for  $\mathcal{C}_{ij}$  is complicated. We simplify it into two sub-problems that can estimate  $H_L, H_U$ , and  $R$  separately. We reason that the probability of the glider being in  $\mathcal{C}_{ij}$  in the  $z$  direction is greater than  $1 - \alpha$  and the probability of it being within the horizontal cross section of  $\mathcal{C}_{ij}$  is greater than  $1 - \alpha$ , i.e.,

$$\begin{cases} \Pr\{H_L \leq H \leq H_U\} \geq 1 - \alpha \\ \Pr\{D \leq R\} \geq 1 - \alpha \end{cases} \quad (5)$$

With (5), given a specified  $\alpha$ ,  $H_L, H_U$ , and  $R$  can be estimated using statistical inference theory [17] by relying on the available  $N$  samples.  $H_L$  and  $H_U$  can be solved as the lower and upper bounds of the two-sided confidence interval of  $H$ , while  $R$  can be solved as the bound of the one-sided confidence interval of  $D$ . The samples of  $H_n$  (for  $H$ ) and  $R_n$  (for  $D$ ) can be calculated from the available  $N$  position samples  $loc_n$ . As shown in the Appendix, we have the following two propositions.

*Proposition 2:*  $H_L$  and  $H_U$  are estimated by

$$\begin{cases} H_L = \bar{H} - \hat{t}_{\alpha, N-1} S^{(H)} \sqrt{1 + 1/N} \\ H_U = \bar{H} + \hat{t}_{\alpha, N-1} S^{(H)} \sqrt{1 + 1/N} \end{cases}, \quad (6)$$

where  $\bar{H} = \sum_{n=1}^N H_n / N$  is the mean of the current  $N$  samples,  $S^{(H)} = [\frac{1}{N-1} \sum_{n=1}^N (H_n - \bar{H})^2]^{1/2}$  is the unbiased standard deviation, and  $\hat{t}_{\alpha, N-1}$  is the 100(1 -  $\alpha/2$ )% of *Student's t-distribution* [17] with  $N - 1$  degrees of freedom.

*Proposition 3:*  $R$  is estimated by

$$R = \frac{\sqrt{N-1} S^{(R)}}{\sqrt{\hat{\chi}_{\alpha, 2(N-1)}}}, \quad (7)$$

where  $S^{(R)} = [\frac{1}{N-1} \sum_{n=1}^N (R_n - \bar{R})^2]^{1/2}$ ,  $\bar{R} = \frac{1}{N} \sum_{n=1}^N R_n$ , and  $\hat{\chi}_{\alpha, 2(N-1)}$  is the 100(1- $\alpha$ )% of  $\chi$ -distribution with  $2(N-1)$  degrees of freedom.

As shown in Fig. 4(a), the greater  $\Delta$  is, the bigger the estimated cylinder is. Glider  $i$  receives  $j$ 's update messages less frequently when  $j$  moves farther away since it may need other gliders to relay these messages, therefore,  $C_{ij}$  will become larger. As the number of position samples becomes smaller,  $f$  will become larger and  $j$ 's position estimation will become less accurate, according to Fig. 4(c). For this uncertainty, deterministic geographic routing may be a problem, while our solution offers higher success rate to forward packets to the destined glider by using a statistical region.

### C. Cross-layer Optimization

After the unicast regions are estimated, a glider needs to select an appropriate neighbor to forward each packet to its intended destination. As mentioned in the previous section, the harsh underwater communication environment makes it necessary to adopt a cross-layer design.

It is shown that today the major part of available energy in battery powered gliders is devoted to propulsion [19], therefore, acoustic communications should not take a large portion of the available energy. Our proposed protocol minimizes energy spent routing a message to its destination as a necessary constraint of UW-ASN, and consider the functionalities of a real acoustic modem for a practical solution. Our protocol employs only local information to make routing decisions, resulting in a scalable distributed solution. The unicast regions obtained in Sect. IV-B are used to select the neighbor with minimum packet routing energy consumption.

To be more specific, given some message  $m$ , glider  $i$  jointly selects a neighbor  $j \in \mathcal{N}_i$ , transmission power  $P_{TX} \in [P_{min}, P_{max}]$ , packet type  $\xi \in \Xi$ , and number of frames  $N_F \in \Omega_\xi$ , so that the estimated energy  $E_{id}$  of routing  $m$  to destined glider  $g_d$ 's region  $C_{id}$  is minimized and forwards  $m$  to it. Here  $\mathcal{N}_i$ ,  $\Xi$ , and  $\Omega_\xi$  denote the set of  $i$ 's neighbors, the set of packet types, and the set of number of type  $\xi$  frames, respectively. We assume power control is possible in the range  $[P_{min}, P_{max}]$  though transmission power is currently fixed for the WHOI Micro-Modem. We anticipate more advanced amplifier hardware will make this power optimization possible.

Here,  $E_{id}$  is estimated by the energy to transmit the packet to neighbor  $j$  in one transmission, the average number of transmissions  $\hat{N}_{TX}^{(i,j)}$  to send  $m$  to  $j$ , and the estimated number of hops  $\hat{N}_{hop}(j, C_{id})$  to region  $C_{id}$  via  $j$ . Let  $L_m(\xi)$  be  $m$ 's length in bits depending on packet type  $\xi$ , and  $B(\xi)$  be the corresponding bit rate. The energy to transmit the packet to neighbor  $j$  in one transmission can therefore be approximated by  $P_{TX} \cdot \frac{L_m(\xi)}{B(\xi)}$ .

Overall, the optimization problem can be formulated as

### $P_{layer}^{cross}$ : Cross-layer Optimization Problem

**Find:**  $j^* \in \mathcal{N}_i, P_{TX}^* \in [P_{min}, P_{max}], \xi^* \in \Xi, N_F^* \in \Omega_\xi$

**Minimize:**  $E_{id} = P_{TX} \cdot \frac{L_m(\xi)}{B(\xi)} \cdot \hat{N}_{TX}^{(i,j)} \cdot \hat{N}_{hop}(j, C_{id})$  (8)

**Subject to:**  $L_m(\xi) = L_F(\xi) \cdot N_F + L_H$ ; (9)

$$\hat{N}_{TX}^{(i,j)} = \frac{1}{1 - PER(SINR_{ij}, \xi)}; \quad (10)$$

$$SINR_{ij} = \frac{P_{TX} \cdot 10^{-TL(l_{ij}, f_c)/10}}{\sum_{k \in \mathcal{A} \setminus \{i\}} P_{TX}^{(k)} \cdot 10^{-TL(l_{kj}, f_c)/10} + N_0}; \quad (11)$$

$$\hat{N}_{hop}(j, C_{id}) = \frac{l_{i, C_{id}}}{\hat{l}(i, j, C_{id})}, \quad (12)$$

where,

- $L_F$  is a frame's length of type  $\xi$ , and  $L_H$  is the length of  $m$ 's header.
- $\hat{l}(i, j, C_{id})$  is the projected distance of line segment from  $i$  to  $j$  on that from  $i$  to  $C_{id}$  while  $l_{i, C_{id}}$  is the distance from  $i$  to  $C_{id}$ .
- $PER(SINR_{ij}, \xi)$  is the PER of type  $\xi$  at  $SINR_{ij}$ . Here PER is obtained by our testbed experiments.
- $TL(l_{ij}, f_c)$  is the transmission loss at distance  $l_{ij}$  at frequency  $f_c$  calculated with Urick model (1)
- $\mathcal{A} \setminus \{i\}$  is the set of active transmitters excluding  $i$ , and  $P_{TX}^{(k)}$  is the transmission power of  $k$ .
- $N_0 = \int_{f_L}^{f_U} psd_{N_0}(f, w) df$  is the ambient noise, where  $psd_{N_0}(f, w)$  is the empirical noise power spectral density for frequency band  $[f_L, f_U]$  kHz as in [12].

In this problem, the objective function estimates the energy to send  $m$  to the destination region  $C_{id}$ ; (9) calculates the message's length; (10) and (12) estimate the number of transmissions to  $j$  and the number hops to  $C_{id}$ , respectively. (11) estimates the SINR from  $i$  to  $j$ ; By solving this problem,  $i$  is able to select the optimal next hop so that  $m$  is routed to the destination with the least energy.

This problem can be solved by enumerating  $j$ ,  $\xi$  and  $N_F$ , searching for the optimal  $P_{TX}$  for each combination of  $j$ ,  $\xi$  and  $N_F$ , and then comparing the minimal values for these combinations. The embedded Gumstix motherboard (400 MHz processor and 64 MB RAM) attached to the Micro-Modem is powerful enough to solve such a problem.

## V. EMULATION TESTBED

Our protocol and cross-layer design are closely coupled with the functionalities of Micro-Modem and testbed. Therefore, in this section, we present the physical and logical architecture of our underwater network testbed. Our underwater testbed relies on a multi-input multi-output audio interface installed on a Personal Computer (PC) and can process real-time signals using software. With the help of softwares such as MATLAB, we can precisely adjust the signal gains, introduce propagation delay, mix the acoustic signals, and add ambient noise and interference in real time. Consequently, underwater communication models described in [12] can be emulated. To our knowledge, our testbed is the best so far to emulate underwater communication channel models.

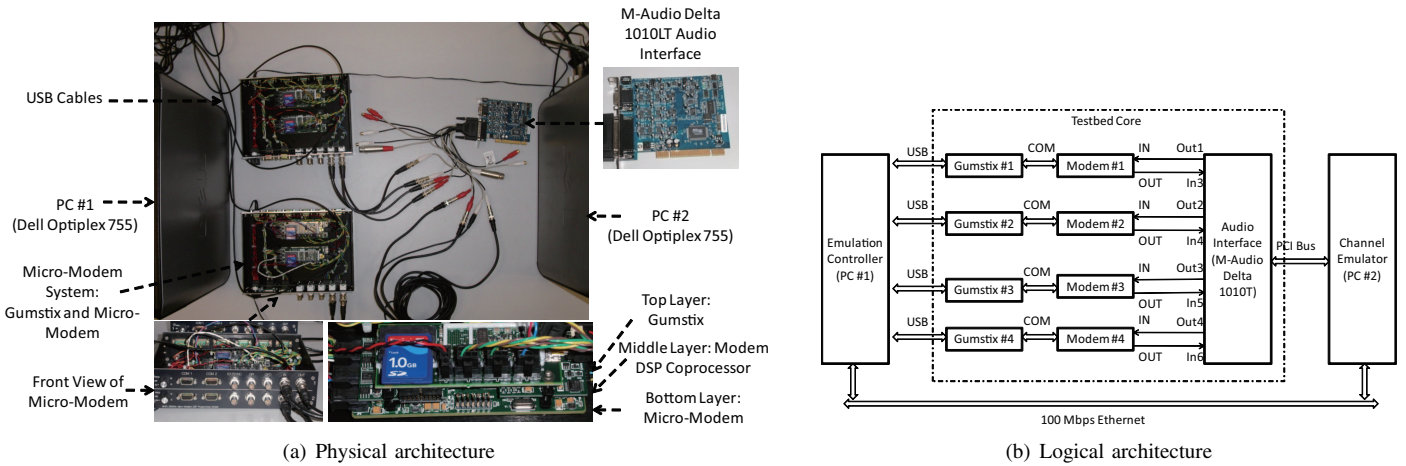


Fig. 5. Testbed architectures.

### A. Physical Architecture

As shown in Fig. 5(a), the physical architecture of our testbed includes the following components.

- **WHOI Acoustic Micro-Modem:** Low-power underwater acoustic Micro-Modem developed by WHOI. It can transmit 4 different types of packets at 4 data rates (Table I) in four different bands from 3 to 30 kHz. Control of the Modem is by NMEA commands [15].
- **Audio Interface:** M-Audio Delta 1010LT PCI Audio Interface [20]. It is a 10-In 10-Out 24-bit PCI audio interface card with maximum sampling rate of 96kHz. It can process the audio signals from multiple inputs in real time and route them to corresponding outputs.
- **Gumstix Motherboard (GM):** The embedded system with Marvell PXA255 400 MHz processor, 64 MB RAM, and 1GB SD disk storage [21]. It runs OpenEmbedded Linux and controls the modem via serial port. It is connected to PCs through the USB port.
- **PC #1:** A Dell Optiplex 755 desktop with Intel 2.4 GHz Quad Core CPU and 2GB RAM. It runs the computer emulation controller software commanding the GMs. It also controls the channel emulator running at PC #2 via Ethernet and collects the emulation results from the GMs.
- **PC #2:** The same configuration as PC #1. It listens to the control information through the Ethernet from PC #1 and emulates the underwater communication channels including signal gain change and ambient noise.

### B. Logical Architecture

The logical architecture of our testbed is shown in Fig. 5(b). When the emulation starts, the Emulation ConTroLler (ECTL) at PC #1 issues commands to the channel emulator at PC #2, which will start emulating the channel according to the parameters provided. ECTL then requests the GMs to run their network tasks. Whenever a packet is transmitted or received, the GMs inform the ECTL via USB connection so that ECTL can collect the emulation results and issue further commands.

Upon the command from PC #1, channel emulator at PC #2 will adjust the gains of input signals, mix them, introduce

propagation delay, add ambient noise, and route the processed signals to corresponding outputs. Acoustic signals are processed in real-time with MATLAB using real-time audio processing package *Playrec* [22].

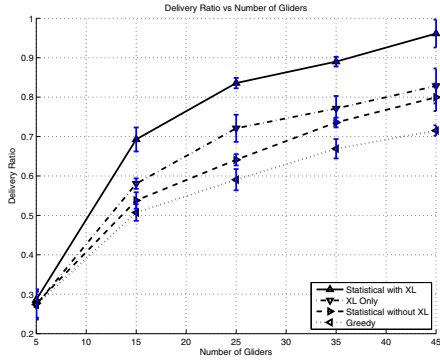
The acoustic gain for each node to node connection is determined in simulation by a Bellhop-based simulator. For each transmitter-receiver pair, a simulation is run to determine the incoherent gain given the transmitter depth, receiver depth, and receiver range. The Munk sound speed profile is used for the simulation because it is a representative open ocean acoustic environment with a depth of 5000 m.

Note that due to the limited number of Micro-Modems and audio processing channels, we can only mix signals from up to 3 transmitters at the receiver modem. Therefore, we calculate, select for transmission, and mix with ambient noise, only the three most powerful signals the receiver will encounter. We leave the simulation of more than three simultaneously transmitted signals as a problem for further research.

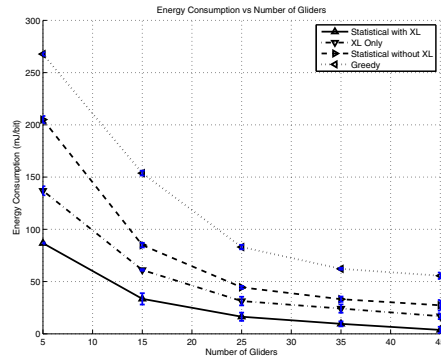
## VI. PERFORMANCE EVALUATION

The communication protocols are implemented and tested on our proposed underwater testbed. We are interested in evaluating the performance of the proposed solution in terms of end-to-end (e2e) reliability, throughput, delay, overhead, and energy consumption under environment that is described by the Bellhop model.

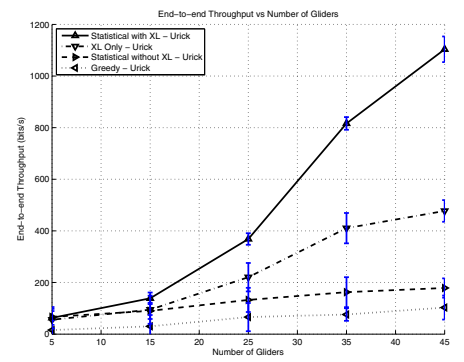
Assume that a glider's drift is a *three-dimensional Brownian Motion* process  $B_t$  ( $t \geq 0$ ) such that, for the glider's present position and  $0 \leq s < t$ , the increment  $B_t - B_s$  is normally distributed with zero mean and covariance matrix  $(t - s)I_3$ , where  $I_3$  is the  $3 \times 3$  identity matrix [23]. As a consequence, the distance traveled by a drifting glider during interval  $\Delta$  is  $3\sqrt{\Delta}$ . Emulation parameters are listed in Table II. Interval  $\Delta$  is chosen to be 30 s in our experiments. As shown in Sect. IV, as  $\Delta$  decreases, the overhead will increase but the estimation of the uncertain region becomes more accurate. Finding a proper  $\Delta$  to balance the tradeoff between overhead and estimation accuracy is left as future work. A glider is randomly selected as the collector and half of the other gliders are randomly selected to



(a) Delivery ratio comparison



(b) Energy consumption comparison



(c) Throughput comparison

Fig. 6. Performance comparison.

TABLE II  
EMULATION PARAMETERS

Parameter	Value
Deployment 3D region	2500(L) $\times$ 2500(W) $\times$ 1000(H)m <sup>3</sup>
Confidence Parameter $\alpha$	0.05
Interval $\Delta$	30 s
$[P_{min}, P_{max}]$	[1, 10] W
Packet Types $\Xi$	{0, 2, 3, 5}
Glider Speed	0.3 m/s
Gliding Depth Range	[0, 1000] m

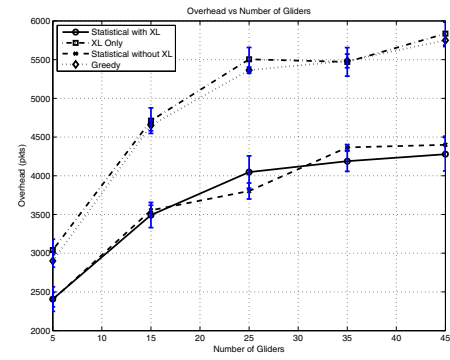


Fig. 7. Overhead comparison.

forward their packets towards it. Emulations are run for rounds and the average is taken for the result.

We are interested in evaluating the performance of our overall solution and different combinations of both the statistical region estimation technique and the cross-layer technique. We also compare them with the deterministic greedy geographic routing protocol, which forwards packets to the neighbor that is closest to the destination. In other words, the protocols we compared are: 1) our proposed solution that combines statistical region estimation and the cross-layer design; 2) protocol with only the proposed cross-layer design; 3) protocol that only uses the statistical region estimation without cross-layer design; 4) protocol that uses deterministic greedy geographic routing. They are denoted by ‘Statistical with XL’, ‘XL Only’, ‘Statistical without XL’, and ‘Greedy’, respectively.

The following e2e metrics are compared:

- **Delivery ratio:** the number of data packets received correctly over the number of total data packets sent;
- **Energy consumption:** the average energy consumed to route one bit of data to the destination;
- **Throughput:** the average bit rate from source to the destination;
- **Overhead:** the average number of overhead packets excluding the data packets;
- **e2e delay:** the average delay to send one data packet from source to destination.

Emulation results are shown in Figs. 6, 7, and 8. The curves are plotted with 95% confidence intervals. The following is

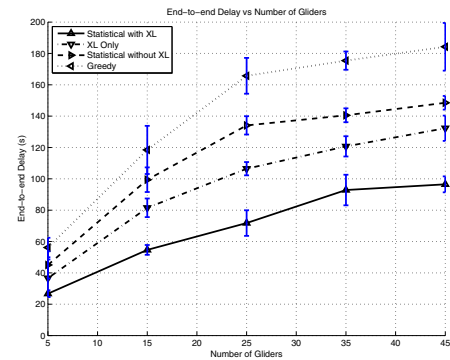


Fig. 8. End-to-end delay comparison.

observed:

- Our proposed solution combining statistical region estimation and cross-layer design achieves the best performance among the above metrics.
- The statistical region estimation and cross-layer components both achieve increased performance over the greedy geographic routing protocol.
- Our solution uses less overhead than ‘Greedy’ and ‘XL Only’ as our solution does not require timely broadcast of the location information for gliders that are two or more hops away.

In sum, statistical region estimation gives higher probability

of forwarding the packets to the destination than only using a deterministic position, and the proposed cross-layer design can minimize the energy consumption to send packets to the destination. By jointly using both components, we achieve increased network performance in terms of delivery ratio, energy consumption, throughput, and e2e delay.

## VII. CONCLUSION

We proposed a trajectory-aware communication solution based on statistical inference for underwater glider networks. The glider regions are estimated using previous locations of the glider with statistical inference methods. Packets are forwarded to the estimated region of the next glider selected by a cross-layer optimization algorithm so that energy consumption is minimized. The whole proposed solution is implemented and tested in our proposed underwater communication testbed, showing improvement over routing protocols with only statistical approach or cross-layer approach and that with deterministic routing in terms of e2e reliability, throughput, and energy consumption.

## REFERENCES

- [1] I. F. Akyildiz, D. Pompili, and T. Melodia, "Underwater Acoustic Sensor Networks: Research Challenges," *Ad Hoc Networks (Elsevier)*, vol. 3, no. 3, pp. 257–279, May 2005.
- [2] E. A. Carlson, P.-P. Beaujean, and E. An, "Location-Aware Routing Protocol for Underwater Acoustic Networks," in *Proc. of IEEE Oceans Conference*, Boston, MA, Sep. 2006.
- [3] J. M. Montana, M. Stojanovic, and M. Zorzi, "Focused Beam Routing Protocol for Underwater Acoustic Networks," in *Proc. of ACM WUWNet*, San Francisco, CA, Sep. 2008.
- [4] D. Son, A. Helmy, and B. Krishnamachari, "The Effect of Mobility-induced Location Errors on Geographic Routing in Mobile Ad Hoc and Sensor Networks: Analysis and Improvement using Mobility Prediction," *IEEE Trans. on Mobile Computing*, vol. 3, no. 3, pp. 233–245, Jul. 2004.
- [5] X. Xiang, Z. Zhou, and X. Wang, "Self-Adaptive On Demand Geographic Routing Protocols for Mobile Ad Hoc Networks," in *Proc. of IEEE International Conference on Computer Communications (INFOCOM)*, Anchorage, AL, May 2007.
- [6] L. Freitag, M. Grund, S. Singh, J. Partan, P. Koski, and K. Ball, "The WHOI Micro-Modem: An Acoustic Communications and Navigation System for Multiple Platforms," in *Proc. of IEEE Oceans Conference*, Washington DC, Sep. 2005.
- [7] P. Bose, P. Morin, I. Stojmenovic, and J. Urrutia, "Routing with Guaranteed Delivery in Ad Hoc Wireless Networks," *ACM Wireless Networks*, vol. 7, no. 6, pp. 609–616, Nov. 2001.
- [8] T. Melodia, D. Pompili, and I. F. Akyildiz, "On the Interdependence of Distributed Topology Control and Geographical Routing in Ad Hoc and Sensor Networks," *IEEE Journal of Selected Areas in Communications*, vol. 23, no. 3, pp. 520–532, Mar. 2005.
- [9] D. Moore, J. Leonard, D. Rus, and S. Teller, "Robust Distributed Network Localization with Noisy Range Measurements," in *Proc. of ACM SenSys*, Baltimore, MD, Nov. 2004.
- [10] D. Pompili and I. F. Akyildiz, "A Cross-layer Communication Solution for Multimedia Applications in Underwater Acoustic Sensor Networks," in *Proc. of IEEE International Conference on Mobile Ad-hoc and Sensor systems (MASS)*, Atlanta, GA, Oct. 2008.
- [11] R. Jurdak, C. V. Lopes, and P. Baldi, "Battery lifetime estimation and optimization for underwater sensor networks," in *IEEE Sensor Network Operations*, S. Phoha, T. LaPorta, and C. Griffin, Eds. Wiley-IEEE Press, 2004.
- [12] M. Stojanovic, "On the Relationship Between Capacity and Distance in an Underwater Acoustic Communication Channel," in *Proc. of ACM International Workshop on UnderWater Networks (WUWNet)*, Los Angeles, CA, Sep. 2006.
- [13] W. S. Burdick, "Underwater acoustic system analysis," in *Prentice-Hall Signal Processing Series*, A. V. Oppenheim, Ed. Prentice-Hall, 1984, ch. 2, p. 49.
- [14] M. Porter, "BELLHOP Gaussian Beam/Finite Element Beam Code," <http://oalib.hlsresearch.com/Rays/index.html>.
- [15] WHOI Acoustic Communications Group, "Micro-Modem Software Interface Guide (Ver 2.98)," <http://acomms.whoi.edu/documents/uModem%20Software%20Interface%20Guide.pdf>.
- [16] J. G. Graver, "Underwater gliders: Dynamics, control and design," Ph.D. dissertation, Princeton University, NJ, May 2005.
- [17] G. Casella and R. L. Berger, *Statistical Inference*, 2nd ed. Duxbury Press, 2001.
- [18] S. J. Ahn, *Least Squares Orthogonal Distance Fitting of Curves and Surfaces in Space*, 1st ed. Springer, 2008, ch. 2, p. 17.
- [19] J. Partan, J. Kurose, and B. N. Levine, "A Survey of Practical Issues in Underwater Networks," in *Proc. of ACM International Workshop on UnderWater Networks (WUWNet)*, Los Angeles, CA, Sep. 2006.
- [20] M-Audio, "Delta 1010LT PCI Audio Interface," [http://www.m-audio.com/products/en\\_us/Delta1010LT.html/](http://www.m-audio.com/products/en_us/Delta1010LT.html/).
- [21] Gumstix Inc., "Gumstix Connex Motherboards," <http://www.gumstix.net/Hardware/view/Hardware-Spec-Sheets/Connex-Spec-Sheet/112.html/>.
- [22] R. Humphrey, "Playrec Version 2.1.1," <http://www.playrec.co.uk/>.
- [23] I. Karatzas and S. E. Shreve, *Brownian Motion and Stochastic Calculus*, 2nd ed. Springer-Verlag, 1991.
- [24] G. Strang, *Linear Algebra and Its Applications*, 3rd ed. Thomson Brooks/Cole, 1988, ch. 7, p. 368.

## APPENDIX

*Proof of Proposition 1:* Computation complexity can be further reduced using the Singular Value Decomposition (SVD) [24],

$$\mathbf{A} = \mathbf{U}\mathbf{\Lambda}\mathbf{V}^T, \quad (13)$$

where  $\mathbf{\Lambda}$  is the diagonal singular value matrix,  $\mathbf{U}$  and  $\mathbf{V}$  are unitary matrices. The columns of  $\mathbf{V}$  are the eigenvectors corresponding to the singular values in  $\mathbf{\Lambda}$ . Hence,

$$\mathbf{A}^T\mathbf{A} = (\mathbf{U}\mathbf{\Lambda}\mathbf{V}^T)^T\mathbf{U}\mathbf{\Lambda}\mathbf{V}^T = \mathbf{V}\mathbf{\Lambda}^2\mathbf{V}^T, \quad (14)$$

which means that the eigenvalues of  $\mathbf{A}^T\mathbf{A}$  are the squares of the singular values of  $\mathbf{A}$ , and the eigenvectors of  $\mathbf{A}^T\mathbf{A}$  are the singular vectors of  $\mathbf{A}$ . Hence the optimal solution  $(a^*, b^*, c^*)$  to the second subproblem in Sect. IV-B is the singular vector of  $\mathbf{A}$  corresponding to its largest absolute singular value. Complexity for this decomposition is  $O(\min(9N, 3N^2)) = O(9N)$  when  $N \geq 3$ .  $\square$

*Proof of Proposition 2:* Assume these  $H_n$ 's are i.i.d. normal variables with the same unknown mean and variance. From predictive inference theory [17], we have

$$\frac{H - \bar{H}}{S^{(H)}\sqrt{1 + 1/N}} \sim t_{N-1}, \quad (15)$$

where  $t_{N-1}$  is the Student's t-distribution with degree of freedom  $N - 1$  with probability distribution function (pdf)

$$f(t) = \frac{\Gamma(N/2)}{\sqrt{(N-1)\pi}\Gamma((N-1)/2)} \left(1 + \frac{t^2}{N-1}\right)^{-N/2}. \quad (16)$$

Here  $\Gamma$  is the well-known *Gamma function*. Solving for  $H$  yields the following distribution

$$\bar{H} + S^{(H)}\sqrt{1 + 1/N} \cdot t_{N-1}. \quad (17)$$

Put this into the second inequality in (5), we can obtain (6).  $\square$

*Proof of Proposition 3:* As stated before, the distributions of the glider's location in the orthogonal  $x, y$  direction of  $C_{ij}$  are i.i.d. normal distributions with  $\sigma_R^2$ . As a result, we have

$$R/\sigma_R \sim \chi_2, \quad (18)$$

where  $\chi_2$  is the  $\chi$ -distribution with 2 degrees of freedom. Let

$$\begin{cases} \bar{R} = \frac{1}{N} \sum_{n=1}^N R_n \\ S^{(R)} = \left[ \frac{1}{N-1} \sum_{n=1}^N (R_n - \bar{R})^2 \right]^{1/2} \end{cases}, \quad (19)$$

we can obtain (7) from [17].  $\square$